ISSN (Print) 1226-1750
ISSN (Online) 2233-6656
Journal of Magnetics 18(2), 105-110 (2013) http://dx.doi.org/10.4283/JMAG.2013.18.2.105

Estimation of Output Voltage and Magnetic Flux Density for a Wireless Charging System with Different Magnetic Core Properties

Ji Hea Park and Sang Woo Kim*

Clean Energy Research Center, Korea Institute of Science and Technology (KIST), Seoul 136-791, Korea

(Received 22 November 2012, Received in final form 27 March 2013, Accepted 1 April 2013)

The design model and key parameters of the material design for the control of induced magnetic flux at the near-field and efficient power transfer in a modified wireless power transfer (WPT) system with a large air gap of wireless electric vehicles were investigated through analytical simulations for magnetic vector and time-domain transient analysis. Higher saturation magnetic core with low core loss induced a stronger vertical magnetic field by the W-type primary coil in the WPT system with a gap of 20 cm at 20 kHz, which is shown from the vector potentials of the magnetic induction. The transient analysis shows that the higher magnetic fluxes through the pick-up cores lead to a linear increment of the alternating voltage with a sinusoidal waveform in the non-contact energy transfer system.

Keywords : wireless power transfer, online electric vehicle (OLEV), electromagnetic field (EMF), magnetic core, output voltage, maxwell simulation

1. Introduction

The Wireless Electric Vehicle (EV) system holds much promise for reducing the demand for the substitution of energy power source. Its potential strongly depends on the capacity of induced electrical power; in particular, focusing between the power line and pick-up module. General research activities in the EV system have increased in recent years from gasoline-based means of transport, causing limited fuel supply. The issue is under active research on battery and inverter, which have proper specifications with cable EV [1-3]. Most of all, the research and development of a wireless electric power transport system are very necessary due to problems with short battery life and causable motive power. Since the past ten years, for this reason, a non-contact power transfer system has been developed [4-8].

However, it is true that a more basic approach to the evaluation of energy transmission efficiency is needed. There are so many efforts involved, such as modification of a circuit component of rectifier or regulator [7, 8], magnetic coupling which induces energy transmission [4-10], magnetic design of core properties [11-13], etc. For the improvement of inductive power efficiency, both the transformed geometrical and electrical factors of the circuit had been applied for the wireless energy transmission systems [14-17]. The configuration of the induced power transfer (IPT) system is very similar to a single phase transformer with an air gap, requiring a large magnetizing current between the primary and secondary coils. Inductive charging makes charging electric vehicles more convenient and creates a lower risk of electrical shock. However, it is hard to solve problems due to its lower efficiency, increased resistive heating, the complexity of the design of inductive charging system, and high magnetic flux leakage during wireless charging.

In an effort to enhance its efficiency and reduce the unnecessary electromagnetic field (EMF), a novel wireless power transfer (WPT) in the on-line electric vehicle (OLEV) has recently been suggested [17-20]. The KAIST-OLEV system has a dual power supply line, from which the magnetic fluxes can transfer doubly. It provides the reduced battery capacity to about 20 percent compared to that of the conventional battery-powered electric vehicles; nevertheless, there is a large air gap of 20 cm between the primary and secondary system. However, endeavors for improving the power efficiency of the non-contact energy transfer system of KAIST-OLEV are still needed in order to achieve the required power transfer capability, due to large leakage inductances.

*Corresponding author: Tel: +82-2-958-5526
Fax: +82-2-958-5529, e-mail: swkim@kist.re.kr

For improved transferring power, the optimal design of material parameters and magnetic flux control in the modified IPT system with a large air gap are very necessary but rarely studied. In particular, the magnetic properties of the iron-based powder cores are a critical factor to enhance the total power output of the secondary coil. Therefore, we investigated the effects of core properties on the output voltage and magnetic flux density in the wireless inductive charging system of KAIST-OLEV.

2. Model Design for a modified WPT system

We used the modified Inductive Power Transfer (IPT) model of the KAIST-OLEV in order to analyze a case excited by a sinusoidal voltage. For controlling the magnetic flux density, we selected Fe-Si powder cores with various permeability values of 26, 60 and 90 μ. Fig. 1 shows the simulation model of the IPT system (1a) consisting of two distinguishing units and a y-z plane view (1b). The developed narrow rail width of IPTS having a large air-gap of 20 cm and a power supply inverter whose input is 60 Hz 3-phase 440 V is proposed for practical applications. The frequency of 60 Hz for the power transfer is converted to 20 kHz at the invert stage. The air gap

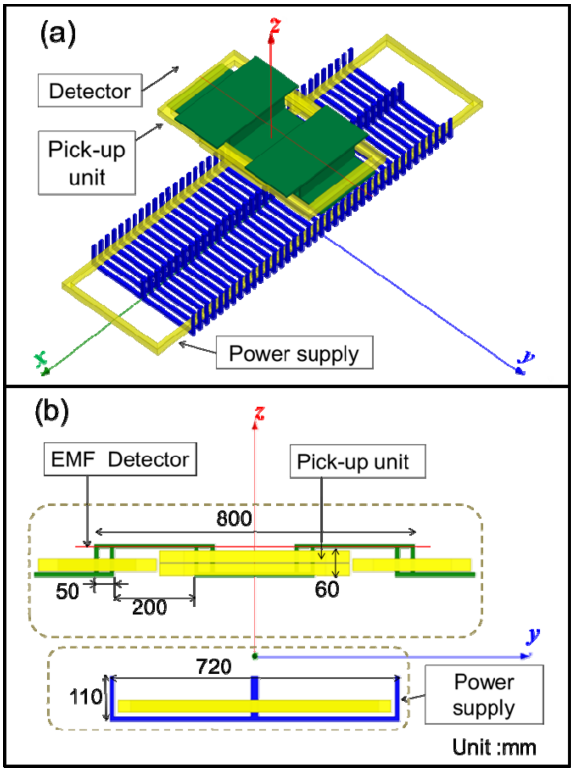

Fig. 1. (Color online) Simulation model of the inductive power transfer system consisting of a pick-up and power supply unit for the wireless electric vehicle.

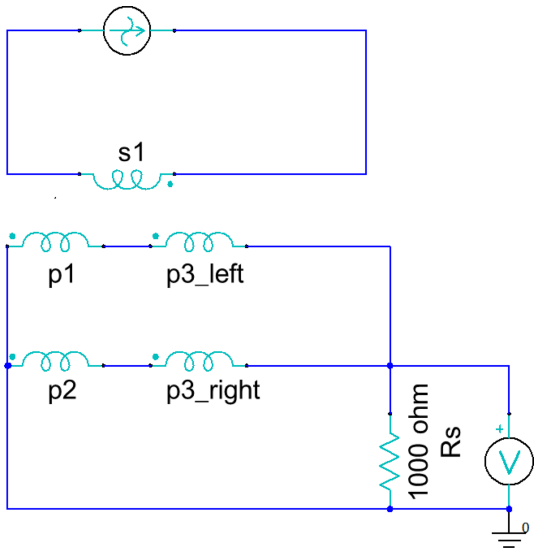

Fig. 2. (Color online) Configuration of the equivalent circuit model of the IPT system.

which can directly affect the field distribution and final output value is set to be 20 cm, corresponding to the distance between the road surface of the W-type primary coil and the bottom surface of the secondary coil part. The magnetic flux is focused in the pick-up unit in order to generate DC power for the vehicle motor. The maximum power is transferred from the power lines under road to the load in the vehicle, and its transfer capability determines the maximum speed and recharging time of the vehicle. The EMF detector, marked with a red color in Fig. 1(b), is located at the uppermost part of the pick-up core plates for magnetic field measurement. Through the eddy current analysis, magnetic flux density distribution data are also observed.

Fig. 2 shows a simplified equivalent circuit model of the IPT system. For the magnetic field analysis using a 3-dimensional eddy current field solver, each loop is applied with a different ampere. Specifically, 260 A is applied to the s1, primary loop. The p1 and p2 loops are applied to 840 A and p3_up and p3_down loops have been applied to an ampere of 960. For acquiring the output voltage data using Maxwell's magnetic transient solver (Ansoft, Ver.11), the applied current in the primary loop is 260 A and the operation frequency is fixed at 20 kHz.

3. Results and Discussion

3.1. Measured material parameters

Fig. 3 depicts the non-linear hysteric nature for magnetic core materials with different initial magnetic permeability. All the magnetic cores exhibit a typical soft mag-

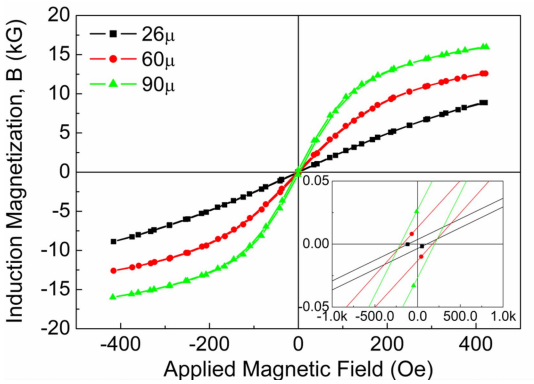

Fig. 3. (Color online) B-H magnetization hysteresis loops of magnetic cores with different permeability values of (a) 26 μ, (b) 60 μ and (c) 90 μ.

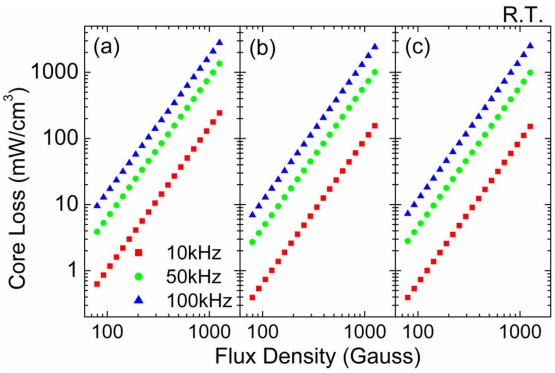

Fig. 4. (Color online) Core loss properties with different permeability values of (a) 26 μ, (b) 60 μ and (c) 90 μ.

netism and the magnetic coercivity is within the range of 109-201 A/m, as shown in the magnified view of Fig. 3. In the B-H curves, as the permeability values increased from 26 to 90, the saturation magnetization (B_S) values of the powder cores linearly increased from 0.86 to 1.58 T at 400 Oe. The measured core loss curves are presented in Fig. 4. The results show a tendency that the saturation magnetizations increase but the core losses slightly decrease at the same operation frequencies, according to the increase in magnetic permeability.

The measured input values of the magnetic powder cores for the numerical analysis of electromagnetic field and output voltage in the IPT system are summarized in Tables 1 and 2. Tables 1 and 2 show the core properties for the simulation of EM field distributions using eddy current solver and the material parameters in order to compute the node voltage levels using the transient solver, respectively. For an accurate modeling and transient analysis, core losses with sinusoidal waveforms in the iron-based magnetic materials were predicted by the Steinmetz equation [21]:

$$P_{Core} = C_m \cdot f^x \cdot B_m^y \quad (1)$$

where C_m is the fitting parameter of the measured power loss, f is the working frequency (Hz), B_m is the peak flux amplitude of the AC flux component (T) of ferromagnetic cores. The C_m, x, and y values, which are fitted from the core loss data, are reported in Table 2.

3.2. Magnetic flux density and magnetic vector potential

Fig. 5 shows the variation of magnetic flux densities vs. distance apart from center, which were observed at the detector located in the uppermost pick-up core plates on the y-z plane of the IPT systems, with different magnetic cores. The magnetic flux densities highly increased with increasing permeability of the magnetic cores. Maximum magnetic flux values of 138.2, 211.8 and 248.3 mT were obtained at the cores with saturation magnetization values

Table 1. Summarized core properties used for the analytical simulation of EM field using the Maxwell 3D eddy current solver.

Sample No.	Relative permittivity	Relative permeability	Electrical conductivity (S/m)	Dielectric loss tangent	Magnetic loss tangent
26 μ	3,852	26	4.20×10^{-2}	5,631.03	0
60 μ	3,540	60	2.16×10^{-3}	1.91	0
90 μ	1,330	90	1.45×10^{-4}	1.21	0

Table 2. Summarized magnetic core properties used for the analytical simulation of the output voltage using a transient solver.

Sample No.	Bulk conductivity (S/m)	Magnetic coercivity (A/m)	Parameters of ferrite core loss			Mass density (kg/m^3)	*Bs* at 400 Oe (T)
			C_m	x	y		
26 μ	4.20×10^{-2}	1.37	602.89	1.12	2.11	6,095	0.86
60 μ	2.16×10^{-3}	2.20	178.24	1.21	2.14	6,364	1.24
90 μ	1.45×10^{-4}	2.52	2.54	4.46	2.13	6,094	1.58

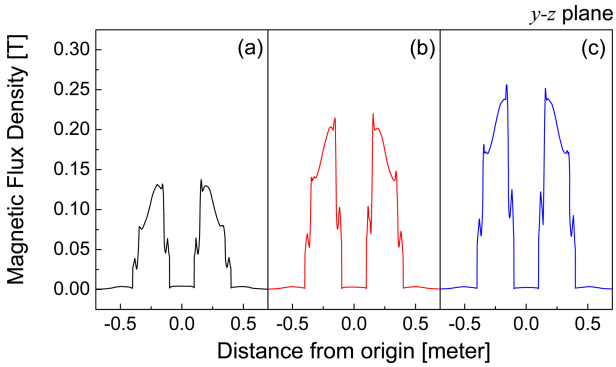

Fig. 5. (Color online) Maximum magnetic flux intensities at the detector located in the uppermost part of the pick-up core plates on the y-z plane of the IPT systems with different magnetic cores.

of 0.86, 1.24 and 1.58 T, respectively. It indicates that the induced magnetic flux is more focused in the pick-up unit at the higher saturation magnetization or permeability. The highest magnetic flux density was observed in the nearby center of the pick-up cores. Fig. 6(a-c) and (d-f) show the 3D magnetic flux density distributions and 2D magnetic vector potentials on the y-z plane of the IPT system with different magnetic cores. We can see that the vector potentials of the left and right sides of the cores are symmetric, yet the directions of the vectors are opposite. The magnetic flux was generated from the power lines with opposite current directions underneath the road surface forming a current loop and was highly focused in the pick-up unit. The huge vertical magnetic flux was caught in the pick-up unit through copper coils around the powder cores. We found in the WPT system that the magnetic flux becomes more focused toward the central parts between the two pick-up cores, as the magnetic saturation increases. It indicates that the magnetic field emitting out of the bus station shrinks considerably.

3.3. Transient voltage analysis

In order to investigate the magnetic saturation effects of the Fe-Si core on generating electric power, generated voltages in the inductive wireless system are compared in

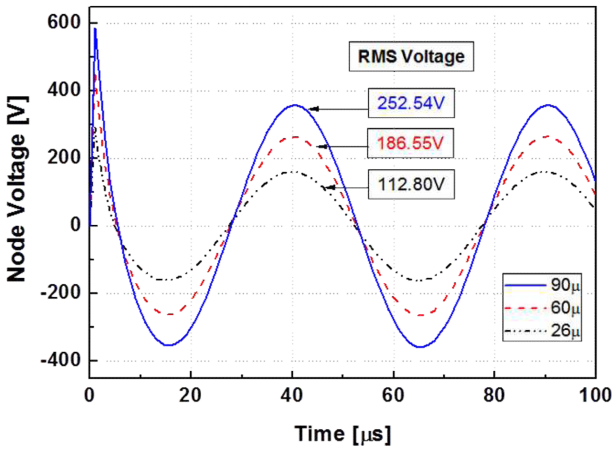

Fig. 7. (Color online) Output voltages for the IPT system with different magnetic cores.

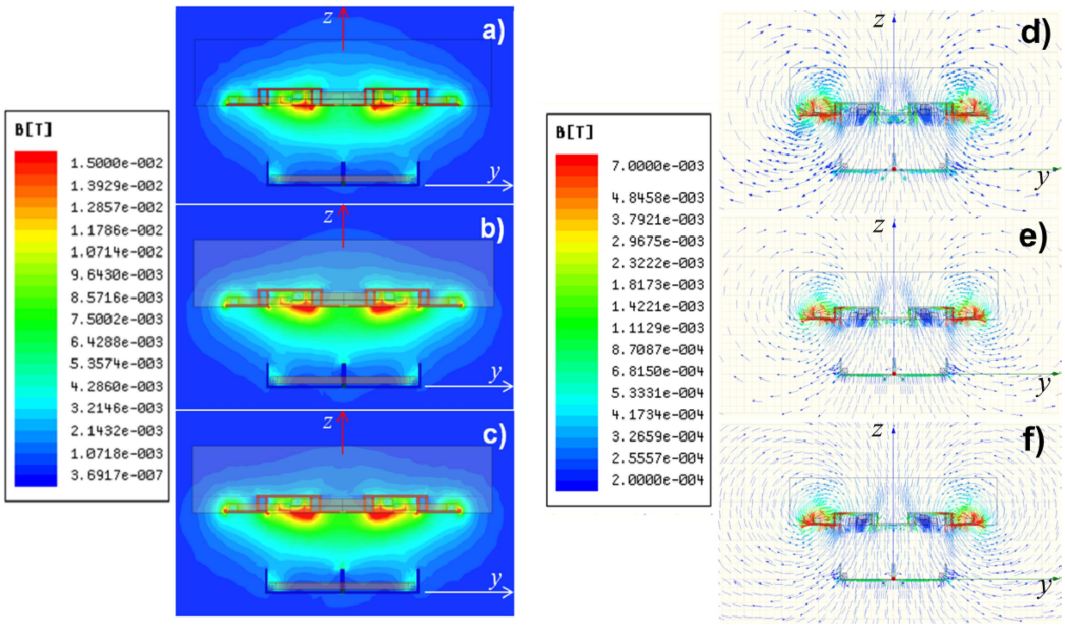

Fig. 6. (Color online) 3D magnetic flux density views (a-c) and (d-f) 2D magnetic field vectors on the y-z plane of the IPT systems with different magnetic cores.

Fig. 7. The AC signals with a sinusoidal waveform were converted to the values of RMS (Root-Mean-Square) voltage. We can see that the RMS voltage values linearly increases as the magnetic saturation (or the relative permeability) gets bigger. In principle, the electric power P_p transferred by this system, is given by [17]:

$$P_p = V_p^2/R_p = (n\omega_s L_m I_s)^2/R_p \quad (2)$$

where V_p is the output voltage, n is the number of turns, ω_s ($=2\pi f$) is the switching angular frequency, L_m is the magnetizing inductance, and I_s is the power supply current. The output voltage of the IPT system is independent on the output current. When f is the frequency, A_{core} is the area of ferromagnetic cores, and B_{core} is the flux density of the ferromagnetic material, and the output voltage V_p is linearly proportional to B_{core} and A_{core}, which is

$$V_p = \omega_s \cdot B_{core} \cdot A_{core} \quad (3)$$

The magnetic flux density of cores only affects the total induced voltage of the secondary coil, because the working frequency and the area of the magnetic core are fixed in this system. In Fig. 7, the transient output voltages show a linear dependency on B_{core}, which are well-consistent with the theoretical prediction of Eq. (3). It indicates that the magnetic saturation of pick-up cores is a critical parameter in focusing the magnetic field induced by the W-type primary coil. The higher magnetic coupling between the primary and secondary is gained by the use of the higher magnetic saturation with low core loss. As a result, the RMS voltage increment to 252.5 V can be achieved when the magnetic powder core with the saturation magnetization of 1.56 T is applied at 20 kHz in the modified WPT system.

4. Conclusion

In this paper, we have presented the key parameters on material design for the control of the induced magnetic flux at the near-field and efficient power transfer in a modified inductive power transfer system with a large air gap of wireless electric vehicles. The proposed design approaches were verified through the numerical simulation of the EM field using Maxwell 3D eddy current solver and transient solver. The magnetic vector potentials indicate that the vertical magnetic field focusing is induced in the pick-up cores with higher saturation magnetization by the primary coil for the modified WPT system with a large air gap of 20 cm at 20 kHz. Time-domain transient analysis shows that the huge vertical magnetic fluxes lead to the enhanced output voltage with a sinusoidal waveform of which the RMS values are linearly proportional to the saturation magnetization of the magnetic powder cores with low core loss in the WPT system of KAIST-OLEV.

Acknowledgments

We gratefully acknowledge financial support from the Korea Evaluation Institute of Industrial Technology and are also grateful to the Korea Institute of Construction & Transportation Technology Evaluation and Planning for partial support of this work.

References

[1] X. Zhang, S. H. Yang, and H. Knickle, J. Power Sources **128**, 331 (2004).
[2] F. Sun, X. Hu, Y. Zou, and S. Li, Energy **36**, 3531 (2011).
[3] F. A. Fleming, P. Shumard, and B. Dickinson, J. Power Sources **78**, 237 (1999).
[4] G. A. Covic, J. T. Boys, and H. G. Lu, 1st IEEE Conference on Industrial Electronics and Applications, May, 1 (2006).
[5] J. L. Villa, J. Sallan, A. Llombart, and J. F. Sanz, Applied Energy **86**, 355 (2009).
[6] M. Jufer, N. Macabrey, and M. Perrottet, Mathematics and Computers in Simulation **46**, 197 (1998).
[7] S. Satoshi and S. Takahide, European patent EP 2 333 932 A1 (2011).
[8] C. S. Wang, O. H. Stielau, and G. A. Covic, IEEE Transactions on Industrial Electronics **52**, 1308 (2005).
[9] G. A. Covic, G. Elliott, O. H. Stielau, R. M. Green, and J. T. Boys, PowerCon 2000 International Conference on Power System Technology **3**, 79 (2000).
[10] K. H. Kim, D. W. Hwang, H. S. Park, K. I. Woo, and Y. H. Cho, J. Magn. Magn. Mater. **272-276**, 695 (2004).
[11] W. Chandrasena, P. G. McLaren, U. D. Annakkage, R. P. Jayasinghe, D. Muthumuni, and E. Dirks, Electric Power Systems Res. **76**, 634 (2006).
[12] R. A. Salas and J. Pleite, J. Appl. Phys. **107**, 09A517 (2010).
[13] F. de Leon and A. Semlyen, IEEE Trans. Power Delivery **10**, 315 (1995).
[14] C. S. Jeong, T. I. Sung, K. H. Lee, S. G. Hong, and I. H. Park, International Conference on Electrical Machines and Systems (ICEMS), 1 (2011).
[15] O. H. Stielau and G. A. Covic, PowerCon 2000 International Conference on Power System Technology **3**, 85 (2000).
[16] Y. Matsuda, H. Sakamoto, H. Shibuya, and S. Murata, J. Appl. Phys. **99**, 08R902 (2006).
[17] J. Huh, S. W. Lee, W. Y. Lee, G. H. Cho, and C. T. Rim, IEEE Transactions on Power Electronics **26**, 3666 (2011).
[18] S. Y. Ahn, H. J. Lee, J. G. Byun, D. S. Kang, T. Song, Y. B. Chun, J. H. Yim, D. H. Cho, and J. H. Kim, 32nd Annual Meeting The Bioelectromagnetics Society (BEMS), 2010.

[19] S. W. Lee, J. Hur, C. B. Park, N. S. Choi, G. H. Cho, and C. T. Rim, Energy Conversion Congress and Exposition (ECCE), 2010 IEEE 1598 (2010).
[20] S. Ahn, J. Y. Lee, D. H. Cho, and J. Kim, CIRP Design Conference 233 (2011).
[21] K. Venkatachalam, C. R. Sullivan, T. Abdallah, and H. Tacca, Accurate Prediction of Ferrite Core Loss with Nonsinusoidal Waveforms Using Only Steinmetz Parameters 8th IEEE Workshop on Computers in Power Electronics, June, 1 (2002).